Mine Water and the Environment (2021) 40:520–538
https://doi.org/10.1007/s10230-021-00777-z

TECHNICAL ARTICLE

Evaluation of Groundwater Inflow into an Iron Mine Surrounded by an Imperfect Grout Curtain

Weichi Chen[1] · Wenping Li[1] · Qiqing Wang[1] · Wei Qiao[1]

Received: 15 March 2020 / Accepted: 1 April 2021 / Published online: 26 April 2021

Abstract
Grout curtains are often used to manage lateral water inflow. However, grout curtains constructed in extremely fractured rocks are not very effective, which poses a challenge for mine drainage and mining operations. So, it is crucial to consider the curtain's effectiveness when evaluating water inflow. Large-scale pumping tests and groundwater numerical simulation were used in this study to evaluate the water inflow at an iron mine surrounded by an imperfect grout curtain. The effectiveness of the curtain was determined by comparing the hydraulic differences on both sides of the curtain and flow fields at pre- and post-grouting stages and three preferential seepage paths were identified. Given the mine's complex boundary conditions, the telescopic mesh refinement modeling method was used; regional and local models were established using FEFLOW. The predicted inflow due to the gap in the curtain was 13,880 m^3/day, accounting for 37.1% of the total 37,340 m^3/day of water that still flowed into the mine. Two countermeasures, surface curtain remediation and underground grouting, were used to decrease water inflow and restore mine productivity.

Keywords Large-scale pumping test · Numerical simulation · Mine water · FEFLOW

Introduction

Most of China's metal mines exist in aquifers and the water inflow exceeds 10^5 m^3/day. These mines have proven reserves of 3.26 billion metric tons (t) and account for 67.7% of the total reserves (Guo 2005). To maintain dry working conditions and improve mining safety, the groundwater is drained before exploitation, which triggers a series of environmental problems including land subsidence (Tzampoglou and Loupasakis 2018), farmland damage (Candeias et al. 2015; Huang et al. 2014), reduced flow from springs and rivers (Liu et al. 2019; Qiao et al. 2017), and ecosystem deterioration (Yang et al. 2019). To increase protection of water resources and environment, the installation of grout curtains, as a vertical hydraulic barrier, has been adopted, such as at the Zhongguan iron mine (Zhang et al. 2016) and Gaoyang iron ore mine (He et al. 2012). Construction of the curtain allows the groundwater inside the barrier to be rapidly drained and protects the water resources outside of the barrier.

The mine curtain is formed by injecting a massive amount of grout into the rock fissures under a designed grout pressure using surface grout holes. The grout effectiveness is controlled by multiple factors. According to a series of scaled model tests, Zhang et al. (2011) found that grout effectiveness decreased with an increase in groundwater flow rate. Carter and Dershowitz (2012) concluded that the aperture size and connectivity of fissures were the main controlling factors for grout effectiveness. And obviously, complex geology and hydrodynamic activities should reduce a mine curtain's effectiveness.

However, it is difficult to determine the effectiveness of a mine curtain as it is hidden underground, which complicates water inflow prediction. To simplify the study, some numerical simulation investigations have assumed an impervious curtain and assigned a small permeability of 10^{-9} m/day, which exaggerated the curtain blocking effectiveness (Ta et al. 2019; Wang et al. 2017; Zhou et al. 2010). Although many methods have been proposed to predict and assess water inrush risks, such as numerical simulation (Chen et al. 2020), the AHP-EWM algorithm method (Hu et al. 2019),

✉ Wenping Li
Wpli1965@163.com

[1] Institute of Mine Water Hazards Prevention and Controlling Technology, School of Resources and Geosciences, China University of Mining and Technology, Xuzhou 221116, Jiangsu, China

and the three maps-two predictions method (Wu et al. 2016, 2017), studies of water inflow in areas with a mine curtain are scarce.

The objective of this study was to evaluate water inflow into an iron mine, considering the effectiveness of curtain grouting. First, two large-scale pumping tests were performed at pre- and post-grouting stages with the aim of evaluating the hydrogeology of the iron mine and inspecting the curtain blocking effectiveness, respectively. Ascertaining the hydraulic properties of faults and fracture zones can provide guidance for mine curtain construction. Subsequently, two scaled numerical simulation models were established, and a regional model was used to specify the boundary conditions and initial hydrological parameters for the local model. The error statistics of mean absolute error (MAE), Nash–Sutcliffe (NS) coefficient of efficiency, and Morris sensitivity analysis were used to evaluate the simulations' accuracy and stability. Finally, the mine water inflows with and without the curtain were predicted, and the curtain's effectiveness was evaluated in terms of decreased water inflow. As a large amount of groundwater still flowed into the iron mine, two potential countermeasures are proposed and discussed.

Hydrogeological Site Framework

Geographical Setting

The study site is in Lujiang county, Anhui province, at approximately 117° 29′ E, 31° 07′ N, which belongs to the Huangtun River valley basin. As shown in Fig. 1, the regional topography is higher in the north, west, and east, where the hills have elevations of 50–400 m above sea level. The groundwater flows through the mined area from south to north and finally drains into the Tian River. The Huangtun River, a tributary of the Tian River, is recharged by precipitation and groundwater. Most of the rain infiltrates into the confined aquifers through the exposed bedrock. The studied iron mine is set in a farming region of the middle valley, at an average elevation of 10 m, where the terrain is gentle, flat, and open. The study area is characterized by a typical subtropical humid monsoon climate featuring hot and rainy conditions in summer, and cold and dry conditions in winter. Annual mean precipitation averages 1258 mm, and the mean evapotranspiration is 953 mm.

Geological and Hydrogeological Site Framework

The study area belongs to the Lujiang-Zongrong volcanic basin, which is one of the main mineral basins in the middle and lower Yangtze River area. This area has abundant reserves of iron, sulfur, copper, lead, zinc, aluminum and other minerals. The iron mine is a large hydrothermal deposit, which mainly consists of pyrite, along with iron, copper, gold, and other minerals.

The mine wall strata consist of sedimentary and volcanic rocks. The volcanic rock hosts a series of mineral bodies (Fig. 2). The volcanic rock mainly includes trachyandesite, hornblende trachyandesite, and gravel trachyandesite, which belong to the Jurassic Longmenyuan formation (J_3l). As extrusive rock, J_3l contains many apertures and fissures, which have high transmissivity and contain an abundance of water. The hydraulic conductivity of volcanic rock ranges from 1.04 to 5.27 m/day (Table 1), and there are some zones where the hydraulic conductivity exceeds 10 m/day due to tectonic movement (Supplementary Table 1). The trachyandesite porphyrite of the Jurassic Anshan formation (J_{3a}) is an intrusive metamorphosed rock with less conductivity (0.1–0.14 m/day) than trachyandesite. The Longmenyuan formation, which is more than 300 m thick, is a significant confined aquifer that can pose mine safety problems.

Above the volcanic strata, the surface is covered by quaternary strata (Q_4) composed of plastic clay interbedded with a 18.5 m thick sand-gravel phreatic aquifer layer. With an average depth of 5.7 m, the quaternary aquifer has a hydraulic conductivity ranging from 0.16 to 0.24 m/day and low water abundance but is recharged by bedrock aquifers. Underlying the Jurassic strata are a 28 m thick marlite from the Triassic Lalijian formation (T_3l) and quartz sandstone from the Tongtoujian formation (T_2t). The marlite contains many karst caves and fractures, which has a high conductivity (1.07–1.49 m/day) and contains abundant water. The quartz sandstone, which may be more than 300 m thick, has a low conductivity (0.08–0.27 m/day) and is the oldest strata discovered by drilling.

In the volcanic strata, geophysical prospecting and drilling exploration found five fracture zones (Fp1, Fp2, Fp3, Fp4, and Fp5), and four faults (F_1, $F_{2\text{-}1}$, $F_{2\text{-}2}$, and F_3). The fracture zones were mainly composed of tectonic breccia with developed tensional fissures where massive amounts of drilling fluid leaked during drilling. Obviously, permeable fracture zones would form preferential seepage paths and increase the hydraulic connectivity of the groundwater. Fault F_1, located in the western part of the iron mine, is a tensional reverse fault. Destroyed by fracture zones Fp2, Fp3, and Fp4, the middle segment of F_1 is permeable; the north segment is weakly permeable whereas the south segment is impermeable. Faults $F_{2\text{-}1}$ and $F_{2\text{-}2}$, located in the eastern portion of the iron mine, are tensional normal faults. Drilling cores show that the tectonite is well cemented, so $F_{2\text{-}1}$ and $F_{2\text{-}2}$ were defined as impermeable faults. Fault F_3, located in the northern part of the mine, was defined as a permeable fault due to developed fissures and intense silicification. The permeability assessments of the faults and fracture zones were

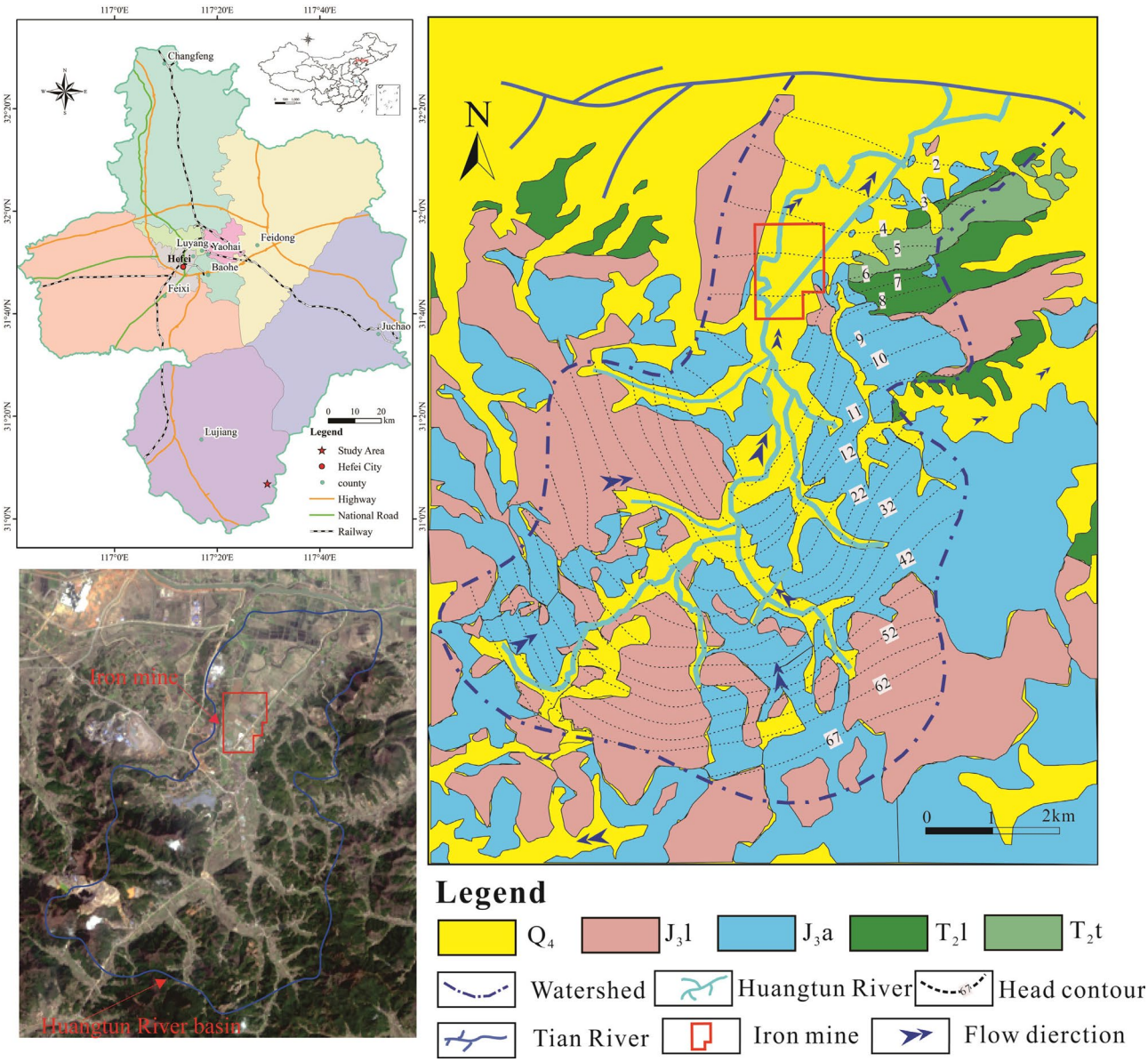

Fig. 1 Position and landform of the study areas

verified by two large-scale pumping tests. The features of the faults and fracture zones are shown in Supplementary Table 2.

Overview of the Mine Components and Grout Curtain

A total of 81 ore bodies of various sizes were detected in the volcanic rock at the interface between the Jurassic and Triassic strata by drilling exploration. The orebodies are characterized by high grade, great thickness, and concentrated distribution. The deposit, with a length and width of approximately 1400 and 450 m, is estimated to contain 40 million t of pyrite, 270 t of iron, 480 t of copper, and 282 thousand troy ounces of gold. The subsurface backfill mining method is being used, and the working faces were set at three elevations (− 140, − 240, and − 340 m). The main shaft and auxiliary shaft were both located in the southeast area of the mine and the roadways were excavated at − 240 m elevation (Fig. 3). To provide dry working conditions and ensure subsurface mining safety, the groundwater table should be decreased to − 240 m, which would result in an immense drainage expense and a huge waste of regional groundwater.

To manage lateral hydraulic recharge to the mine, a large-scale mine curtain was constructed and was connected to the

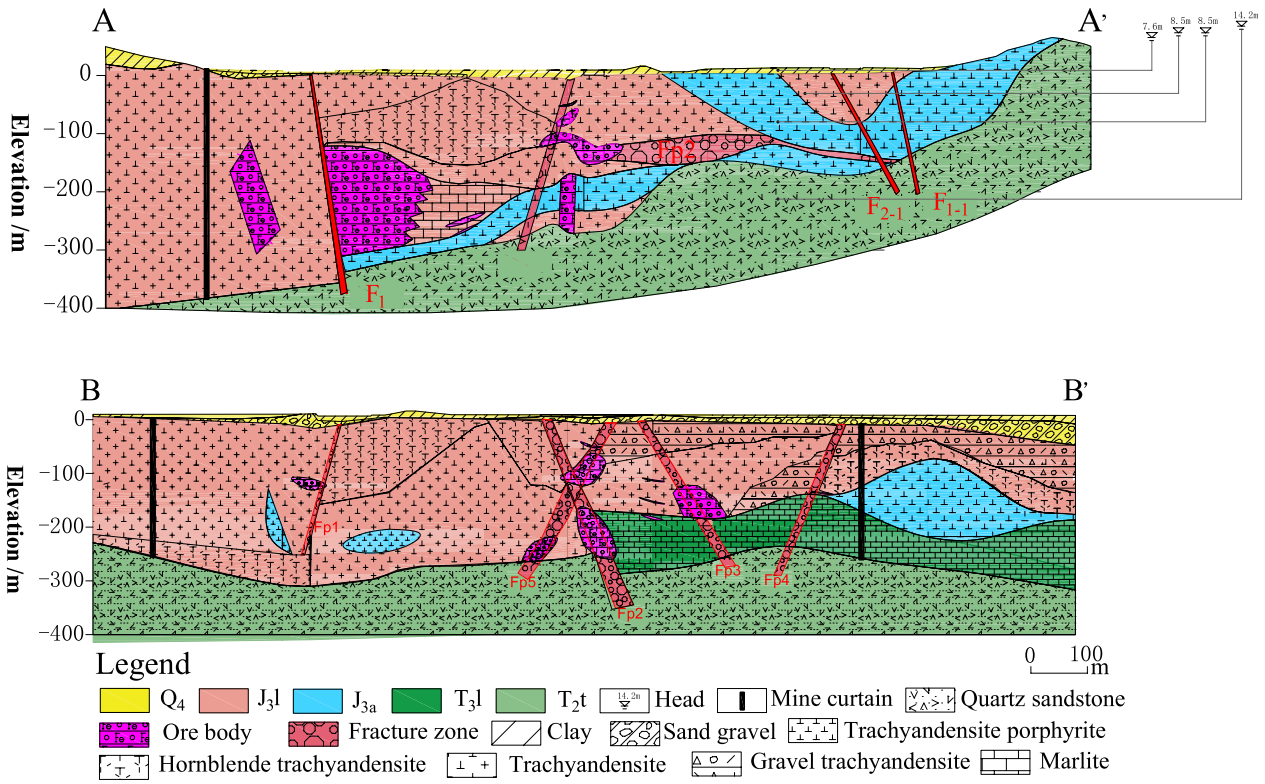

Fig. 2 Geological profile of study area

Table 1 Geological and hydrogeological property of strata in study area

Stratigraphic unit	Name of strata	Type rock	*E* (m)	*BD* (m)	*T* (m)	*K* (m/day)	*q* (L/s m)	Hydraulic test[a]
Q_4	Clay	Sedimentary rock	9.2	0.5	3.3–9.2 (6.5)	0.16–0.24	0.01–0.33	4
	Sand gravel		2.2	7	0–50 (18.5)			
	Clay		− 16.3	25.5	3–29 (17.6)			
J_3l	Trachyandesite	Volcanic rocks	− 33	372	56–98 (73)	1.04–5.27	0.13–16.5	10
	Hornblende trachyandesite				87–126 (107)			
	Gravel trachyandesite				76–135 (97)			
	Trachyandesite porphyrite	Intrusive rock			18–67 (46)	0.1–0.14		
T_3l	Marlite	Sedimentary rock	− 390	400	23–35 (28)	1.07–1.49	11.64–16.79	2
T_2t	Quartz sandstone		− 418	428	> 300	0.08–0.27	0.07–0.08	2

J_3l Longmenyuan formation, T_2t Tongtoujian formation, T_3l Lalijian formation, *E* elevation of layer surface (m), *BD* buried depth of layer surface (m), *T* layer thickness (m), *K* hydraulic conductivity (m/day), *q* unit water inflow (L/s m)

[a]See Supplementary Table 1

natural impermeable faults to form an underground enclosed barrier. However, no curtain was built in the mine's southeast section due to construction difficulties and land expropriation problems. Thus, the mine curtain was not fully enclosed. The construction of the mine curtain, with a horizontal length of 2722 m, took 32 months and cost more than 180 million RMB. The curtain extended vertically into the Triassic quartz sandstone strata at a mean depth of 293 m to block the hydraulic connection within the volcanic rock and marlite aquifers. As shown in Fig. 3, the zone enclosed by the mine curtain was the first mining area whose orebody reserve reached 20.97 million t. A total of 374 grout holes, spaced 5 m apart, were drilled

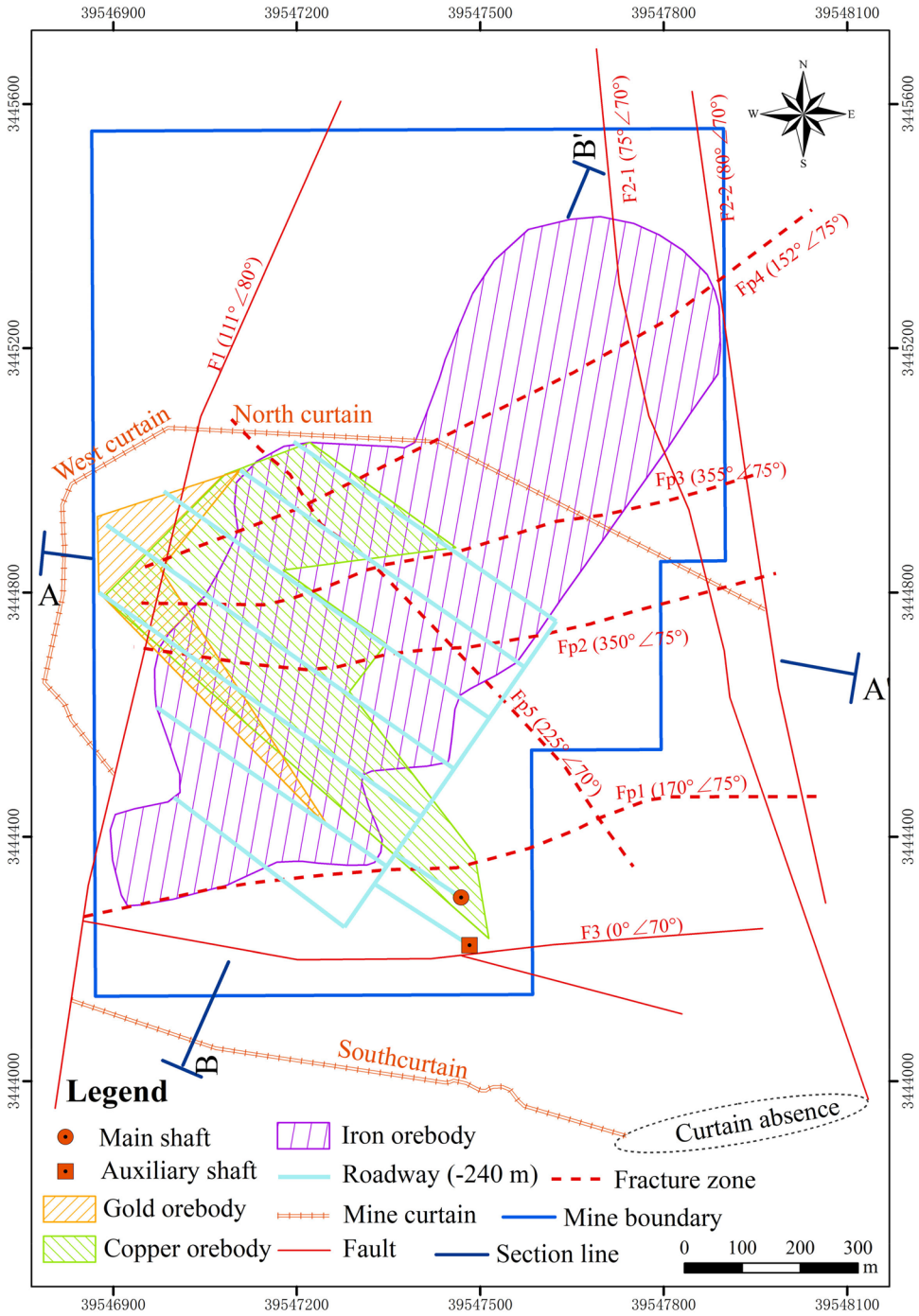

Fig. 3 Plan view of the study area

and classified as primary and secondary holes in two rows, respectively. If the grouting pressure of secondary grouting did not achieve the target criteria, tertiary holes were drilled as complementary holes. The estimated radius of grouting was 6 m to ensure a curtain thickness of 12 m. The drill holes were grouted in 20 m stages using the downstage method (Davis and Horswill 2002) with a target grout pressure of 2.5–4 times the hydrostatic pressure. The average injection amount per meter decreased from 7 m^3 of primary grouting to 3 m^3 of secondary grouting, dropping by 57%. Packer permeability tests from 20 test holes showed that the permeability of the rock mass decreased from 35 Lugeons (4×10^{-6} m/s) at primary grouting to 10 Lugeons (1.1×10^{-6} m/s) at secondary grouting, indicating that the fissures of the aquifer were mostly sealed.

Methods

Field Experiments

The field experiments included two large-scale pumping tests. In Oct. 27, 2012, a pumping test before grouting (PTBG) was conducted. In Feb. 9, 2017, the pumping test after grouting (PTAG) was completed. The objective of PTBG tests was to ascertain the mine hydrogeology and provide a design reference for curtain construction. The PTAG results were used to evaluate the curtain's effectiveness and identify the preferential seepage channels penetrating dysfunctional curtain zones. The depth and diameter of pumping holes BK01 and BK02 were enlarged to increase pumping capacity in the second test. For hole BK02, the depth was increased from 111 to 227 m, and for hole BK01, it was increased to 300 m. The diameter of the holes was increased from 270 to 800 mm (Fig. 4c) and the well screen diameter was increased from 230 to 620 mm to

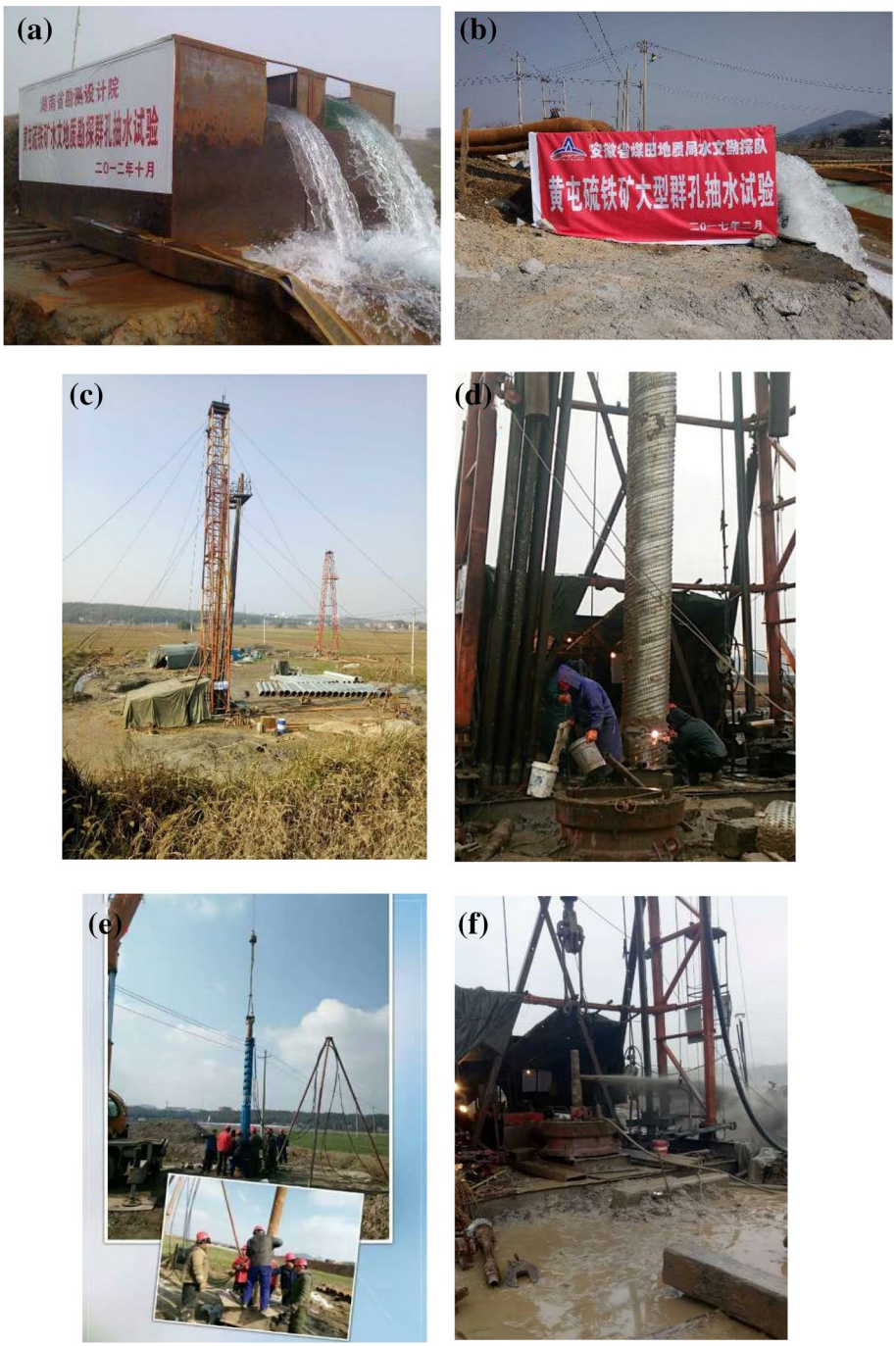

Fig. 4 Construction site of pumping test **a** PTBG test; **b** PTAG test; **c** drilling holes; **d** well screens installation; **e** pump installation; **f** flushing holes

install high-lift pumps (Supplementary Fig. 2 and Figs. 4d and 4e). For observation holes, 130 mm diameter casing pipe was installed in the quaternary clay layer; no screen was installed in the bedrock where the hole diameter was 90 mm. In addition, the holes were flushed using an air compressor to satisfy the test requirements (Fig. 4f). The flowrate was calculated using the water table height in a rectangular water discharge box, which was measured twice daily (Fig. 4a, b). The experimental time for the PTBG was 23 days, including 9 days of pumping and 14 days of recovery. The largest drawdown in holes BK01 and BK02 reached 20.11 m and 30.5 m, with flowrates of approximately 415 and 184 m^3/h. In the PTAG, the pumping lasted 91 days and the largest drawdown of BK01 and BK02 reached 96 and 106.9 m. With the increased pumping time, the flowrate decreased from 642 to 526 m^3/h for BK01 and from 640 to 454 m^3/h for BK02 (Supplementary Fig. 2).

Artificial water table monitoring using measuring ropes was conducted in two tests involving over 50 workers. The PTBG monitoring network included 34 observation holes in the confined aquifer and eight holes in the quaternary aquifer, which were mainly distributed on both sides of the faults and nearby fracture zones. Due to hole wall collapse, 13 observation holes lost their measurement function and 12 holes outside the curtain were added in PTAG (Fig. 5). The water table drawdown of observation holes in two tests are shown in Supplementary Table 3. Four observation holes were located on both sides of the middle segment of fault F_1 (BK03, ZK2203, GK08, and GK16), with drawdowns of 10.28, 9.53, 10.23, and 10.07 m in PTBG, which indicated that the fault segment was permeable. Three observation holes were located on both sides of the north segment of fault F_1 (GK18, BK06, and BK07) with drawdown of 3.68, 8.09, and 7.62 m in PTBG, indicating that fault segment was slightly permeable. In PTAG, the drawdown of hole G15 was 1.53 m which suggested that the south segment of fault F_1 was impermeable. Simultaneously, holes GK04, BK06, and GK09 indicated that fault $F_{2\text{-}1}$ was weakly permeable, and $F_{2\text{-}2}$ was impermeable. There was no large hydraulic difference for observation holes on both sides of F_3 and fracture zones. Hence, they were defined as permeable structures.

Numerical Simulation

Analysis of the iron mine hydrogeology based on the PTBG hydraulic test showed that there were no natural barriers to block the north and south lateral water flow. Faults $F_{2\text{-}1}$ and $F_{2\text{-}2}$ can block east flow, whereas F_1 can only block part of the west underground water. Despite the mine curtain, there was still partial water inflow into the mine. Since the boundary inflow amount could not be calculated precisely, the telescopic mesh refinement method (TMR) was adopted for the numerical simulation of transient-state pumping tests, in which a larger encompassing regional model is used to specify the boundary conditions and initial hydrological parameters for a smaller embedded local model (Leake and Claar 1999; Ward et al. 1987; Hunt et al. 2001). As a result, two scaled numerical models were established using the software package FEFLOW (DHI-WASY 2017; FEFLOW version 7.1), where the regional model encompassed the entire Huangtun River valley basin and the local model comprised the iron mine and surrounding zones. In the regional model, the Tian River was taken as the specified head boundary and the watershed was taken as the zero-flux boundary (Fig. 6a). The Huangtun River was assigned as the GHB boundary, which is hydraulically connected with the Q_4 layer. In the local model, the southern and northern boundaries were defined as specified flux boundaries with values obtained from the regional model. Fault $F_{2\text{-}2}$ and part of the watershed were selected as the east and west zero-flux model boundaries (Fig. 6b). In the upper and bottom interfaces, the model was recharged by precipitation and a deeper sandy layer, respectively. Based on the vertical distribution of strata, there were four layers that represented the gravel phreatic aquifer and thin clay aquifuge of Q_4, the thick confined aquifer of J_3l and T_3l, and the thick confined aquifer of T_2t, with average thicknesses of 18, 22, 237, and 196 m, respectively. Given the dip of the faults and fracture zones, ranging from 70° to 80°, they were assumed to be vertical structures (90°) to simplify modeling and reduce calculation; their width and length were assigned using Supplementary Table 2. The mine curtain was also assumed to be a vertical structure with a width of 12 m, with parameters assigned according to its effectiveness. Considering the heterogeneity of the water-bearing media in the study area, the FEFLOW triangular elements were used to produce the non-uniform calculation nodes, and some zone meshes were refined. Within the regional model, the embedded model zone and the Huangtun River were discretized by fine grids with area of 115 m^2; the other zone was discretized by coarse grids of 2.45 km^2. As a result, 23,108 grids and 12,548 nodes were produced in a regional model with an area of 40.08 km^2. Within the local model, the surrounding zones of holes, faults, fracture zones, and mine curtain were discretized by fine grids with an area of 5.6 m^2. The other zone was discretized by coarse grids spanning an area of 78 m^2. A total of 71,237 grids addressed the local model area of 3.69 km^2, and 35,818 nodes were produced.

The common approach in constructing a transient-state simulation includes specifying the starting head as the ending head from a steady-state model to eliminate readjustment errors between two groundwater flow states, but some models have ignored this step (Dong et al. 2012). Assuming that groundwater was steady-state flow prior to the pumping, to maintain the consistency of the double

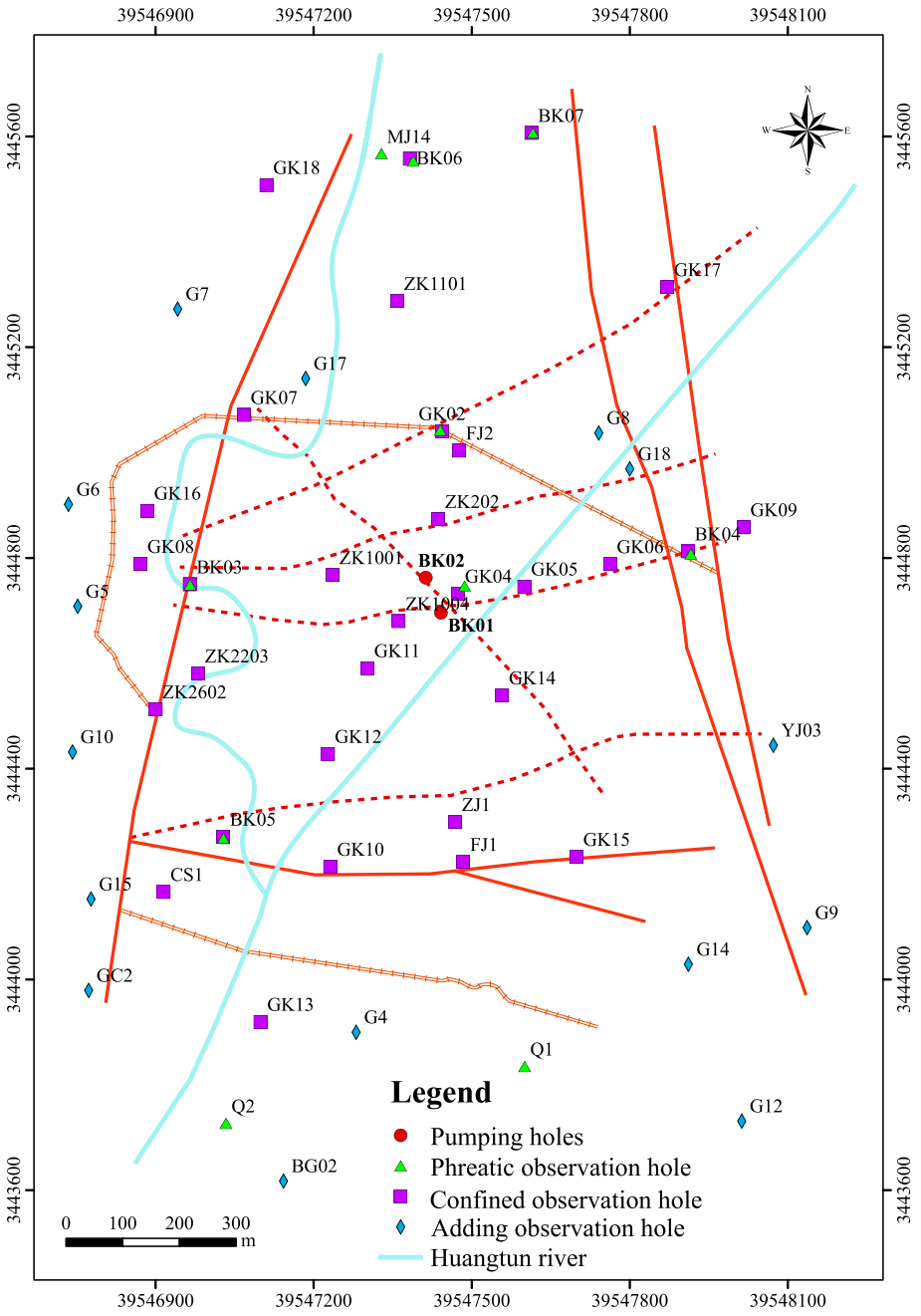

Fig. 5 Arrangement of pumping holes and observation holes

scale transient-state models, the following steps adopted in this case were: (1) simulating steady-state flow without pumping in the regional model; (2) specifying the constant boundary flux for local model from the regional model and simulating steady-state flow in the local model; (3) comparing the water head distribution of the regional model and local model as well as observations; (4) simulating transient-state flow with pumping in the regional model, specifying the starting head as the ending head from a steady-state regional model; (5) specifying the changing boundary flux for local-model from the transient regional model and simulating transient-state flow in the local model to use the ending head from the steady-state local-model simulation as the starting head; and (6) comparing the results of the transient-state local model and regional model as well as observations to verified the modeling reasonability and analyze the grout curtain's effectiveness.

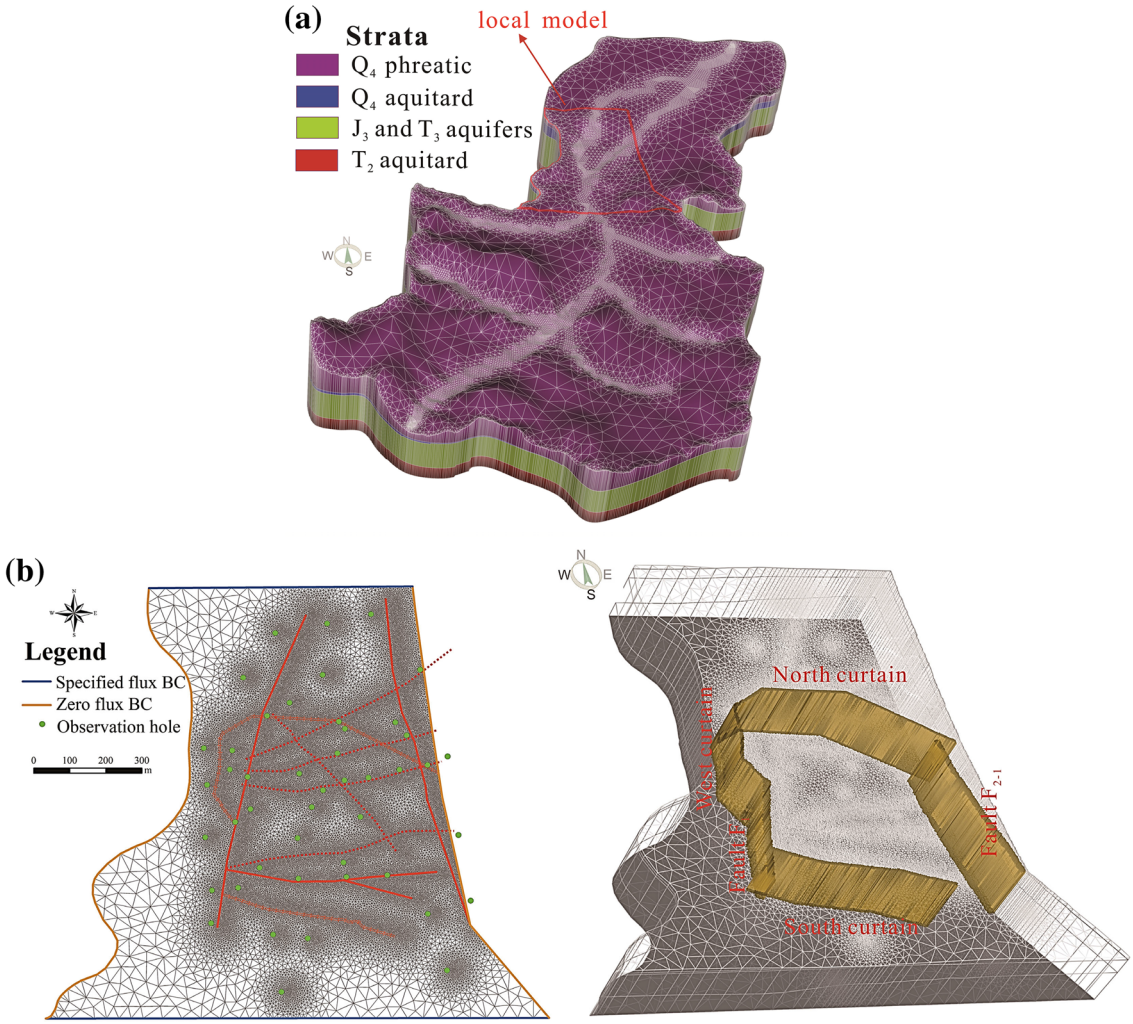

Fig. 6 Two scale numerical simulation model for calculating water inflow into the iron mine **a** regional model; **b** local model

Results

Mine Curtain Evaluation

Pumping tests are useful in identifying potential seepage paths when evaluating the blocking effectiveness of a mine curtain (Medeiros et al. 2010), especially for a large drawdown. By blocking the hydraulic recharge from outside, the curtain increases the hydraulic difference on both sides of it. Thus, the larger the water table difference, the more effective the mine curtain. In PTAG, the changes in the water table of the curtain observation holes is shown in Fig. 7. On both sides of the north curtain, six holes were selected: holes G8, G17, G18, FJ2, GK02, and GK06 (Fig. 7a). Outside the curtain, hole G17 had almost the same water table change as G18, and the drawdown of G8 was larger than that of G17 and G18. Inside the curtain, the hydraulic difference between the observation holes was small, and FJ2 had the lowest water table (− 106.9 m). The hydraulic difference between G8 and FJ2, and G18 and FJ2 reached 7.5 m and 13.7 m, respectively, indicating that the north curtain's middle segment was less effective than the east and west segments. Similarly, the hydraulic difference between holes G6 and BK03, and G10 and BK03 reached 26.3 m and 6.6 m, respectively, indicating that the south segment of the west curtain was less effective than the north segment (Fig. 7b). On both sides of the south curtain, the hydraulic difference between GK13 and GK10 reached 20 m, indicating that the west segment of the curtain was effective. However, G14 had the same drawdown as G12 due to the absence of a curtain in the east side, where groundwater flowed into the mine (Fig. 7c). The flow field contour (Fig. 8a) was plotted manually using mapping software based on observed data in PTAG. For comparison, the corresponding no-curtain flow field was simulated (Fig. 8b). Due to the construction of the mine curtain, the drawdown of water head outside

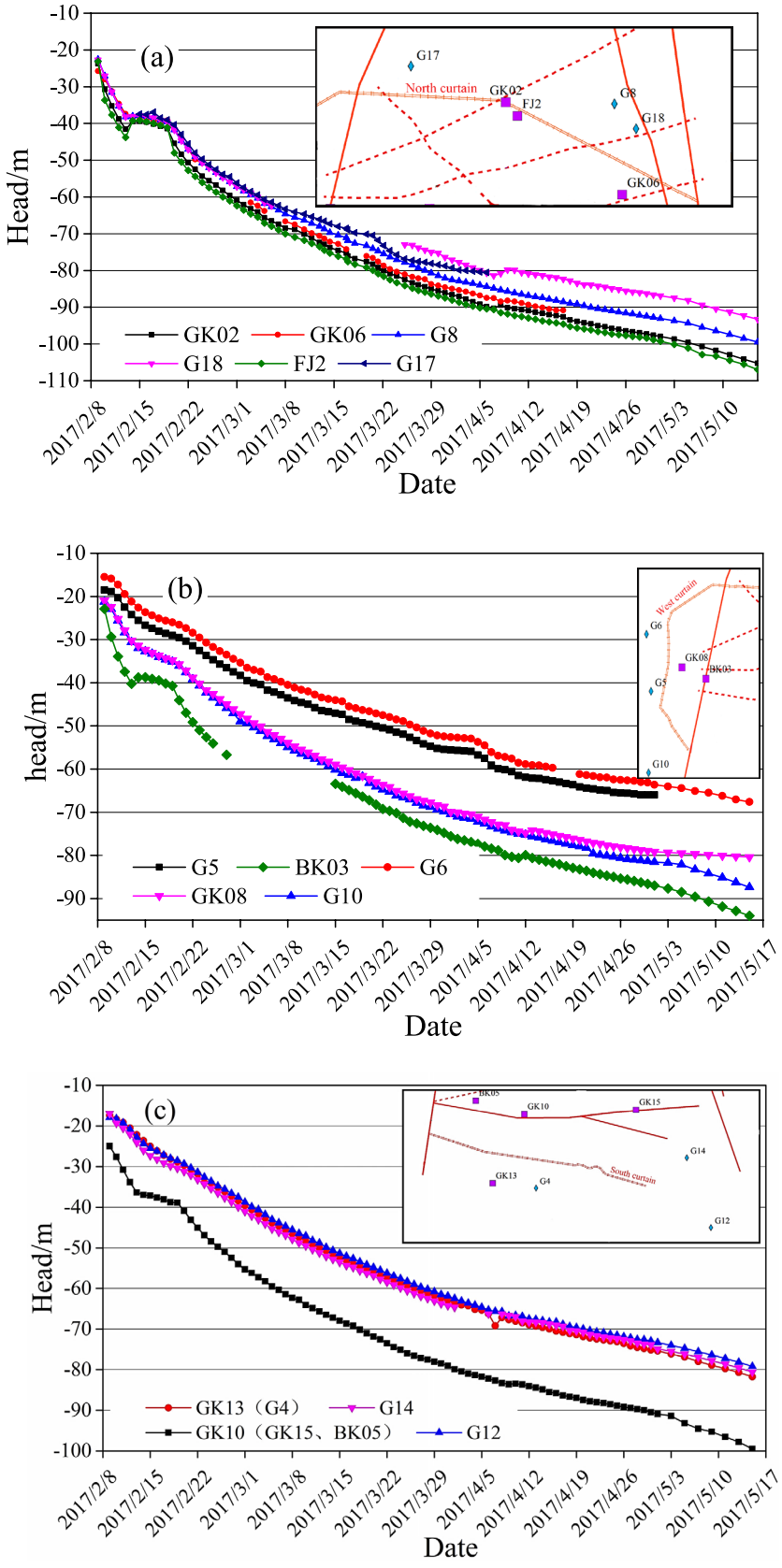

Fig. 7 Hydraulic change on both sides of mine curtain **a** North curtain; **b** West curtain; **c** South curtain

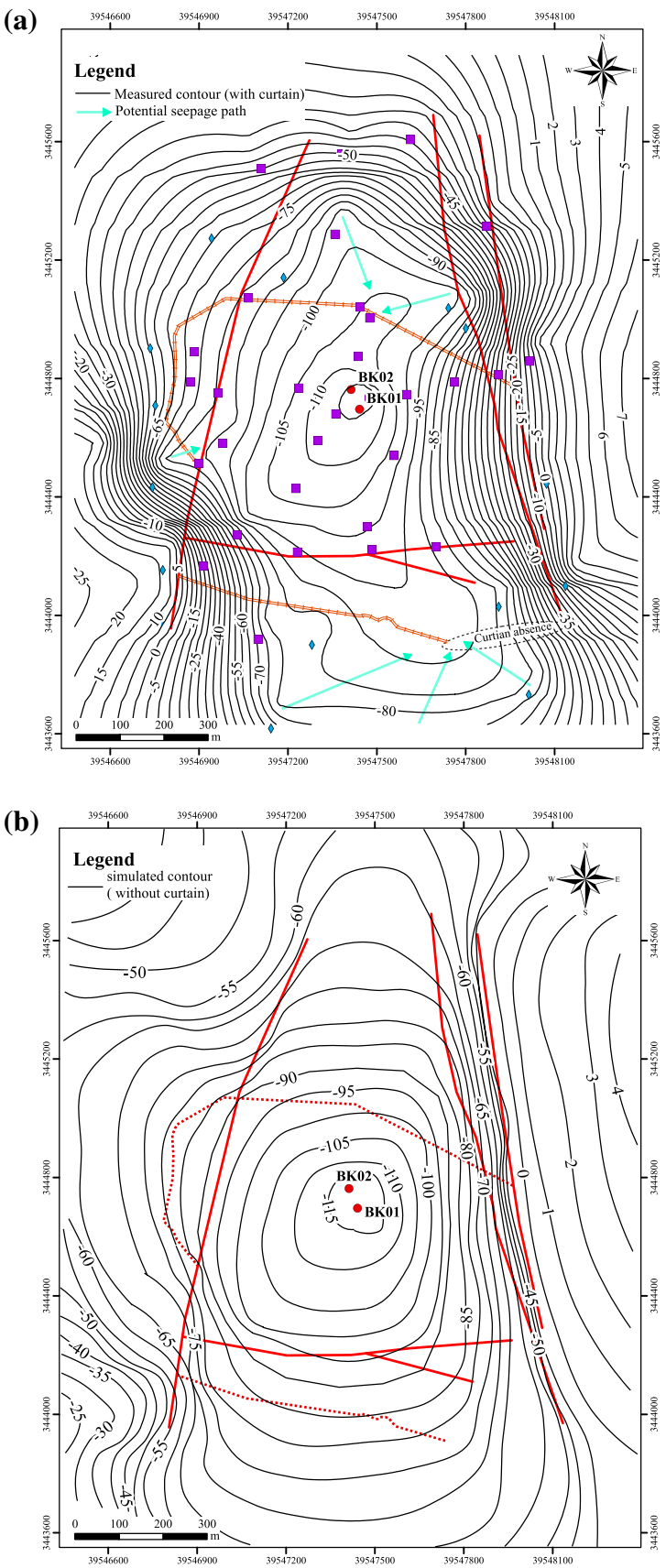

Fig. 8 Flow field comparison of the PTAG test **a** flow field with curtain (measured); **b** flow field without curtain (simulated)

the curtain in Fig. 8a was less than in Fig. 8b, which indicates that the hydraulic gradient was increased on both sides of curtain. The denser the contours outside the curtain, the higher the hydraulic difference, indicating better water-blocking effectiveness. From the contour distribution in Fig. 8a, three catchment paths were determined where the contours were sparse, and their shape protruded to the outside of the mine, forming gradient valleys. The south preferential seepage path was conclusively attributed to the absence of a curtain. The north and west seepage channels were located at the junction between curtain and structures (fault F_1 and fracture zone Fp4). Thus, it is reasonable to deduce that grouting had likely failed in the fractured zones.

Hydrogeological Parameters and Zoning

The parameters obtained from pumping tests can help operators better understand a mine site's hydrogeology, which is the basis of parameter zoning. Based on the measured water table, traditional graphical methods were used to inversely calculate parameters for observation holes (Cooper and Jacob 1946; Theis 1935; Supplementary Table 4). The transmissibility ranged from 74 to 622 m^2/day and the storage coefficient (S_c) ranged from 0.11×10^{-3} to 8.96×10^{-3}, which suggested that some observation holes near permeable faults and fracture zones possessed high conductivity and abundant water. The foregoing steps (1–6) were conducted to simulate pumping tests and the two models were run simultaneously. For consistency, the adjusted parameter values in the local model were also corrected in the regional model. The corresponding boundary conditions extracted from the regional model were interpolated into the local model to form a continuous iteration calculation until the observed water table was calibrated.

The fitted hydrogeological parameters were obtained after many iterations of running model and correcting parameters (Fig. 9a, b; Table 2). The local model was divided into 53 fine parameter zones, which included strata, faults, fracture zones, and curtain, whereas the regional model was divided into 7 coarse zones. Affected by tectonic movement, the permeability of some zones in the local model exceeded that in the regional model, especially for the permeable faults and fracture zones. In the local model, the permeability of zones near structures exceeded that of other zones, such as the pumping holes surrounding zones 1, 2, and 10, with permeabilities reaching 9.22, 8.35, and 7.14 m/day. For fault F_1, the impermeability of the south segment was higher than that of north segment, which showed calibrated permeabilities of 0.07 and 0.41 m/day, respectively. Damaged by fracture zones Fp2, Fp3, and Fp4, the middle segment permeability was higher than that of the host rock, which reached 4.2 m/day. The damage to Fault $F_{2\text{-}1}$ was less than at F_1, which had low permeability (0.07 m/day) in all segments except for a few seepage paths caused by fractured zones. Fault F_3 had no blocking effect and its permeability and specific storage were as high as 4.78 m/day and 5.6×10^{-5}/m. The permeability of the fractured zones was far greater than that of the host rock, ranging from 10.2 to 14.37 m/day, which formed subsurface concentrated seepage belts. In addition, there was abundant groundwater in the fractured zones, which increased the amount of mine drainage. Most segments of the mine curtain had low permeabilities, ranging from 0.26 to 0.58 m/day, which indicated that the volcanic rock fissures were blocked effectively. However, there were permeable zones in the southern segment of the west curtain and the middle segment of the north curtain, such as zones 51 and 48, which overlapped with fault F_1's permeable segment and fracture zone Fp4. The dysfunctional zones formed seepage channels, which allowed groundwater from outside the curtain to flow into the mine. Furthermore, there was a permeability difference between the south curtain and ungrouted zones. Therefore, zones without an effective grout curtain provided a seepage window through which a large amount of water flowed.

Model Error and Sensitivity Analysis

Although numerical simulation of groundwater flow has developed quickly over the last several decades and several guidelines have been published (Murraye Darling Basin Commission 2001; ASTM 2008), universal calibrated criteria have not been adopted by the modeling community for two reasons. First, subjective judgment provides a significant beneficial effect during model calibration. Second, there are many potential modeling targets that require different acceptable error magnitudes (Anderson et al. 2015). Thus, it is impossible to define an appropriately calibrated model with a simple criterion. However, model error statistics can be used to measure the goodness of fit. Here, the MAE and the NS coefficient of efficiency were selected to assess the transient models, which can be calculated using the following equations, respectively:

$$MAE = \frac{1}{\mathrm{n}}\sum_{i=1}^{n}\left|(h_m - h_s)\right|_i \tag{1}$$

$$NS = 1-\frac{\sum_{\mathrm{i}=1}^{n}\left|(h_m - h_s)\right|_i^2}{\sum_{\mathrm{i}=1}^{n}\left|(h_m - \overline{h}_m)\right|_i^2} \tag{2}$$

where n is the measured number of targets; h_m is the observed water table, m; $\overline{h}_m$ is the mean of observed water table, m; and h_s is the simulated water table, m.

The regional simulated flow field NS and MAE errors distribution of the local model as well as the simulated and

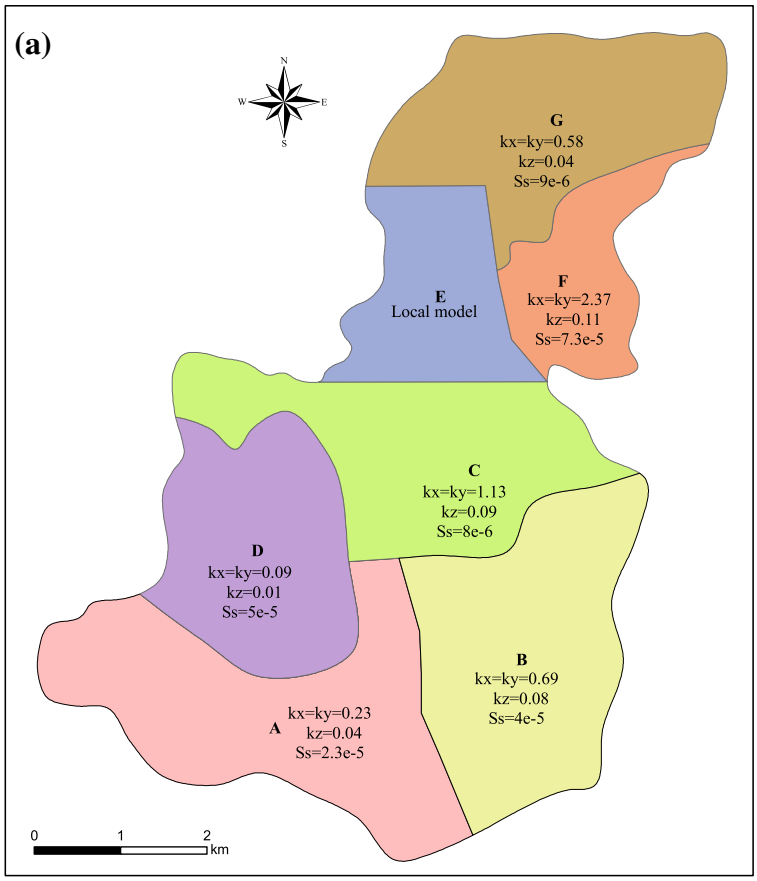

Fig. 9 Parameter zoning of the study area **a** regional model; **b** local model

Table 2 The calibrated parameters of the modeling zoning

Zoning	k (m/day)	S_s ($\times 10^{-5}$/m)	Zoning	k (m/day)	S_s ($\times 10^{-5}$/m)	Zoning	k (m/day)	S_s ($\times 10^{-5}$/m)
1	9.22	1.3	19	3.48	0.64	37	0.41	0.23
2	8.35	1.5	20	1.05	1.12	38	0.07	0.1
3	4.38	1.1	21	0.78	0.5	39	4.2	0.85
4	2.41	1.3	22	0.97	0.5	40	0.07	0.7
5	3.32	0.97	23	1.02	0.5	41	4.78	5.6
6	1.23	1.12	24	1.22	1.24	42	10.2	6.4
7	2.78	0.75	25	3.43	0.86	43	14.37	6.4
8	2.58	1	26	1.12	0.5	44	14.37	6.4
9	3.55	1.14	27	2.21	0.67	45	12.1	6.4
10	7.14	1.7	28	1.2	0.73	46	10.24	5.6
11	1.15	1.22	29	0.98	0.73	47	0.26	–
12	5.07	0.83	30	0.77	0.5	48	8	–
13	3.14	1	31	2.04	1.22	49	0.45	–
14	1.24	0.77	32	1.01	0.84	50	0.26	–
15	1.08	1.15	33	1.56	0.95	51	1.06	–
16	1.88	1.33	34	0.86	0.92	52	0.26	–
17	3.17	0.95	35	1.14	0.77	53	0.58	–
18	2.87	1.1	36	2.05	0.82			

observed water table calibrations of selected holes are shown in Fig. 10a–c. Due to the hydraulic blocking of faults $F_{2\text{-}2}$ and the watershed in east and west segments, the cone of depression caused by mine dewatering mainly extended in north and south, and its propagation distance exceeded 3 km (Fig. 10a). As shown in Fig. 10b, good consistency was maintained between simulated and observed flow fields in the local model. Although the MAE values of some holes were exceeded 1 m, such as hole BK01, most of the holes had only small errors. Moreover, the NS values ranged from 0.85 to 0.95, which indicated that the model was highly accurate. Six holes were selected to compare the simulated and observed water tables, and the absolute error was computed (Fig. 10c); other holes are compared in Supplementary Fig. 3. It was found that the calculated groundwater table was generally consistent with the measured water table.

Sensitivity analysis was used to identify the model's dependence on various input factors, which can determine the most sensitive factor to decrease the calibrated errors (Liu and Li 2019; Zhao 2013). Traditionally, parameter sensitivity can be calculated by the following formula:

$$S_{i,k} = \partial y_i / \partial x_k \approx \left[y_i\left(x_k + \Delta x_k\right) - y_i\left(x_k\right) \right] / \Delta x_k \quad (3)$$

where $S_{i,k}$ is the sensitivity of result i for factor k; y is the function relating to x; x is the original factor; and Δx is the increment factor. Given the multiple parameters in this case, the Morris analysis method (Morris 1991) was adopted and 14 parameter combinations were obtained based on the four controlling factors: the conductivity and specific storage of confined aquifer (K and S_s), the hydraulic conductivity of the grout curtain (K_G), and the boundary fluid-flux of local model (q) (Table 3). When an individual factor or combination varied by 10%, the sensitivity was calculated using Eq. 2 (Xue et al. 2018). As shown in Fig. 11, 10% variability of factors K, K_G, q, and S_c caused water table changes of 0.35, 0.3, 0.22, and 0.16 m, respectively. Thus, conductivity was the principal factor and had the maximum effect on the simulated results. Furthermore, when the four factors were varied by 10% (combination 14), the water table change was only 1.16 m, accounting for 0.97% of drawdown, which confirmed that the model was stable and could be adopted to predict water inflow.

Prediction of Water Inflow

The situation at this iron mine is typical of water hazards in mines in southern China, where drainage of the host aquifer combined with mine curtain construction is necessary to create safe mining conditions and protect groundwater resources. However, a curtain's dysfunctional zones and gaps pose a potential challenge to successful dewatering. The inflow assessment plays a significant role in determining appropriate grout curtain remediation measures. The − 240 m elevation was assigned as the drawdown level in the local model, and the inflow amount penetrating three mine curtains was recorded automatically using FEFLOW. Furthermore, according to the *Technical Guide for Mine Grout Curtains in China* (DZ/T 0285 2015), grouting effectiveness can be calculated by quantifying the water inflow decrease after curtain construction, using the following formula:

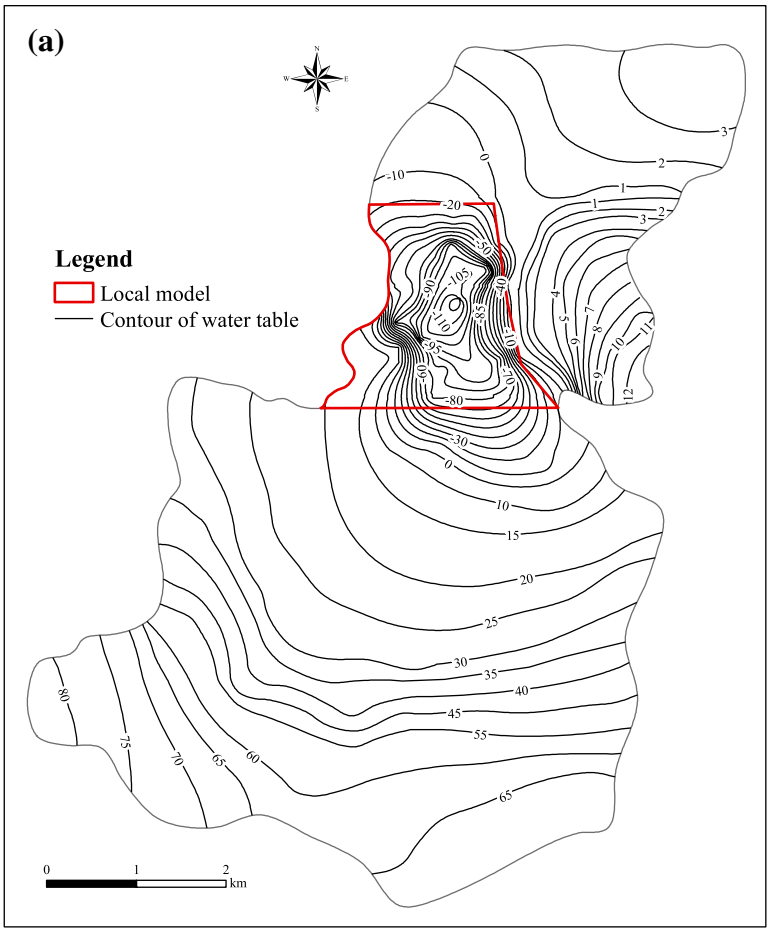

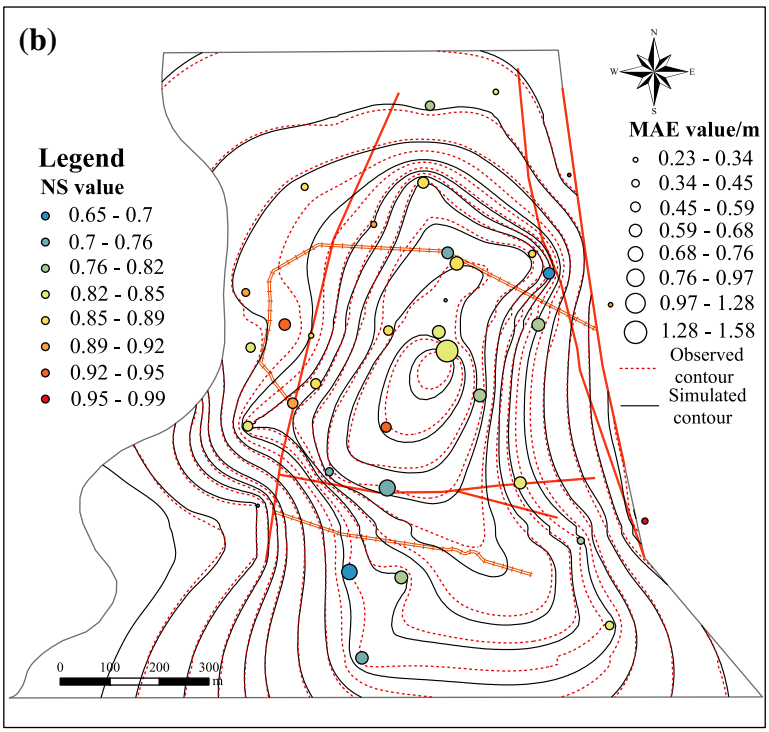

Fig. 10 Calibration and errors statistics of numerical simulation **a** simulated flow field of regional model; **b** NS and MAE errors distribution; **c** water table calibration of selected observation holes

Fig. 10 (continued)

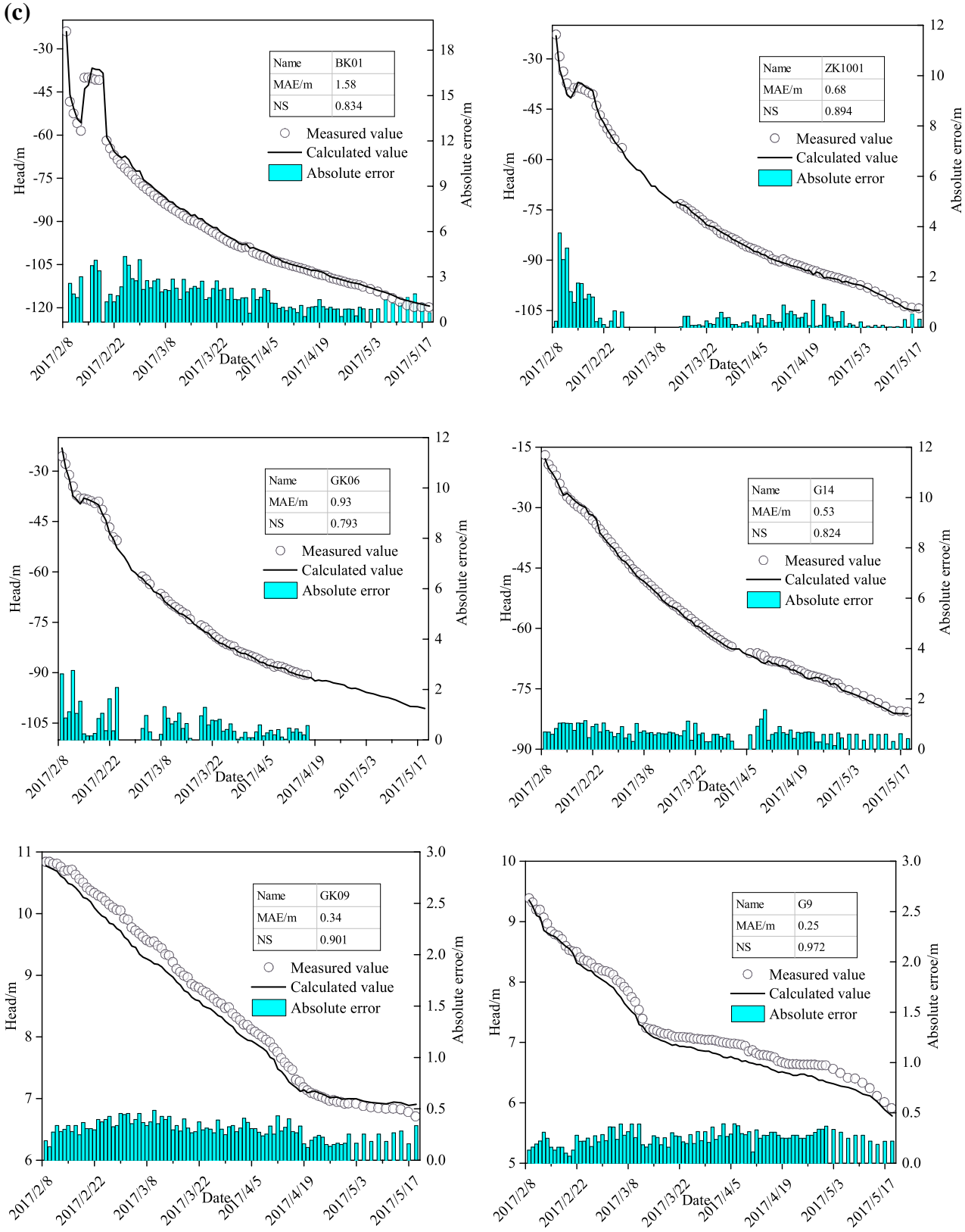

Table 3 Combinations of multiple factors

No.	1	2	3	4	5	6	7
Combination	K	K_G	q	S_S	K, K_G	K, q	K, S_S
No.	8	9	10	11	12	13	14
Combination	K_G, q	K_G, S_S	K, K_G, q	K, K_G, S_S	K, q, S_S	K_G, q, S_S	K, K_G, q, S_S

K the conductivity of confined aquifer (m/day), S_s the specific storage of confined aquifer (1/m), K_G the conductivity of grouting curtain (m/day), q THe fluid-flux of boundary (m^2/day)

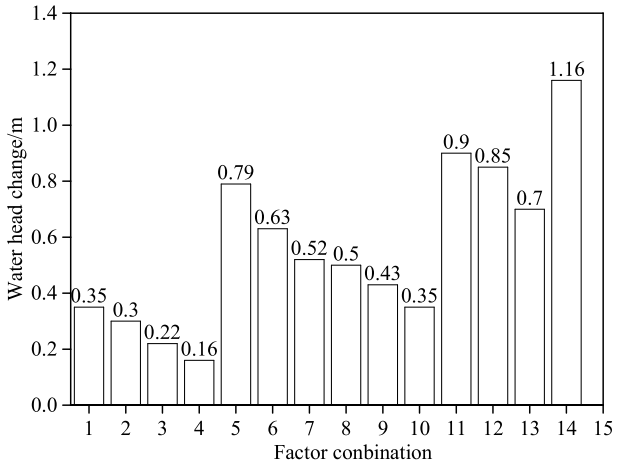

Fig. 11 Sensitivity analysis of multiple factors

$$G_e = \frac{W_b - W_a}{W_b} \tag{4}$$

where G_e is the grouting effectiveness, W_b is the water inflow into the pit before grouting construction, m^3/day, and W_a is the water inflow into the pit after grouting construction, m^3/day. As indicated by Eq. 4, the greater the value of G_e, the easier it is to mine safely. Based on the calibrated regional and local models, the mine inflow amounts under natural conditions (without the curtain) and grouting (with the curtain) were predicted, respectively.

As shown in Table 4, before curtain construction, the predicted water inflow was 121,280 m^3/day. A large amount of groundwater flowed into the mine from the south and north, up to 54,200 m^3/day (zones 52, 53, and 18) and 42,280 m^3/day (zones 47, 48, and 49), respectively. Two factors contributed to this phenomenon. First, north–south was the primary natural groundwater direction of flow, and the iron mine is in a fan-shaped basin seepage outlet. Second, the strong water-bearing volcanic rock aquifer is extremely thick and has substantial water reserves. After curtain construction, only 23,460 m^3/day of water penetrated the curtain and most of the inflow outside the curtain was blocked effectively. Curtain zones 48 and 51 had larger inflow than other zones due to preferential seepage channels in the north and west curtains. The effectiveness of zones 48 and 51 reached

Table 4 Prediction of water inflow and evaluation of blocking effectiveness

Name	Zoning	Inflow (m^3/day)		Decrement (m^3/day)	Effectiveness (%)
		Nature	Grouting		
North curtain	47	13,310	2720	10,590	79.5
	48	15,790	5560	10,230	64.7
	49	13,180	2130	11,050	83.8
West curtain	50	12,520	3520	9,000	71.9
	51	12,280	4300	7,980	64.9
South curtain	52	12,070	1600	10,470	86.7
	53	31,000	3650	27,350	88.2
Absence	18	11,130	13,880	–	–
Total	–	121,280	37,340	83,940	69.2

64.1% and 64.9%, respectively, which was less than elsewhere. Significantly, 13,880 m^3/day of water amount flowed into the mine through the gap in the curtain in the southeast portion of the mine, accounting for 37.1% of the total inflow. Although the comprehensive effectiveness of the curtain reached 69.2%, the inflow still totaled 37,340 m^3/day. Thus, additional measures need to be implemented to achieve proper mining conditions.

Although the effectiveness of a grout curtain can be evaluated by other methods, such as the filling degree of boreholes or packer permeability tests, it was assessed from the water inflow in this study because of the frequent mine water inrush events. Besides, although water inflow may decrease over time in long-term mine dewatering, the predicted results still provide good references for mine water management and curtain remediation.

Discussion

Although most of the groundwater was blocked by the curtain, the predicted mine water inflow reached 37,340 m^3/day when the groundwater was dewatered to − 240 m elevation. A large amount of water resource was still being wasted and the drainage cost was very high. Therefore, surface grouting remediation measures to block the preferential seepage channels in the mine curtain was considered as an option. However, although the horizontal leakage positions of the

north and west curtain were detected by pumping tests, the vertical position of the leaky areas had not been accurately determined. Supplemental field tests, such as micro-seismic monitoring (Mendecki 1997), fluorescent tracers (Battaglia et al. 2016), and electromagnetic computed tomography (ECT) (He et al. 2012), could potentially be used to define the exact leakage depth, but we realized that surface remediation of the grout curtain would still allow most of the inflow to continue.

Therefore, supplemental grouting via an underground roadway was proposed for the ungrouted zones. If the supplemental curtain was 80% effective, the water inflow could be decreased by approximately 11,000 m^3/day. This option was considered more feasible that surface remediation in terms of cost and construction. In addition, additional boreholes surrounding the south and north curtain were proposed to accelerate the dewatering. Also, it was realized the mine curtain may be damaged by mining deformation and the high hydraulic difference, so long-term curtain stability monitoring was also suggested.

Since synthesis exercises in projects of this magnitude are complex, simulation errors still exist, although the model was well calibrated. In this paper, TMR modeling was used. However, there were only two boreholes outside the area of interest within the regional zone, so the calibration of the large-scale model as well as the boundary conditions are likely somewhat inaccurate. There is no doubt two-scale modeling increases the likely error compared with single-scale modeling. However, the lack of information in the regional zone can be resolved, given the large number of mineral mines in this region. If the regional model was well calibrated for the area outside of the iron mine, the boundary condition of the other mineral mines could also be assigned. Thus, the two-scale modeling has a developmental advantage. Meanwhile, an attempt to establish an intermediate-size numerical model to decrease this simulation errors will soon be launched. The simulation mesh will be increased with the existing computational capabilities to investigate how the simulation is influenced by incorporating more calculation nodes.

Conclusions

Large-scale pumping tests and groundwater numerical simulations were performed in this case study to evaluate water flow into an iron mine surrounded by an imperfect grout curtain. Three preferential flow paths flowing through the curtain were identified; two paths were caused by grouting dysfunctional zones and the other seepage path was attributed to the ungrouted zones. Except for the dysfunctional zones, most of the mine curtain had low permeabilities, ranging from 0.26 to 0.58 m/day, which can block groundwater effectively.

Despite the mine curtain, 37,340 m^3/day of water flowed into the mine, of which 37.1% flowed through the ungrouted zones. Two countermeasures, surface curtain remediation and underground grouting, were proposed to decrease water inflow. An 80% effective supplemental curtain would decrease water inflow by ≈ 11,000 m^3/day. In addition, roadway release drill-holes surrounding the south and north curtains were proposed to accelerate the dewatering, as well as long-term curtain stability monitoring. These measures were all adopted, and now the iron mine is operating and productive. This case study of inflow evaluation of an imperfect grout curtain may be beneficial for mine water management and grout curtain remediation elsewhere.

Supplementary Information The online version contains supplementary material available at https://doi.org/10.1007/s10230-021-00777-z.

Acknowledgements Financial support for this work was provided by the Fundamental Research Funds of the State Key Program of National Natural Science of China (Grant No.41931284), and the National Basic Research Program of China (Grant No.2015CB251601). The authors also thank the reviewers for their useful comments.

References

Anderson MP, Woessner WW, Hunt RJ (2015) Applied groundwater modeling: simulation of flow and advective transport. Academic Press

ASTM (International) (2008) Standard guide for calibrating a groundwater flow model application D5981-96. American Society of Testing and Materials. ASTM International

Battaglia D, Birindelli F, Rinaldi M, Vettraino E, Bezzi A (2016) Fluorescent tracer tests for detection of dam leakages: the case of the Bumbuna dam Sierra Leone. Eng Geol 205:30–39

Candeias C, Ávila PF, Ferreira SE, Paulo JT (2015) Integrated approach to assess the environmental impact of mining activities: estimation of the spatial distribution of soil contamination (Panasqueira mining area, central Portugal). Environ Monit Assess 187(3):135–158

Carter TG, Dershowitz W (2012) Improved methods of design for grouting fractured rock. In: Grouting and deep mixing, geotechnical special publications (GSP), vol 28, pp 1472–1483

Chen WC, Li WP, Qiao W, Li LF (2020) Beneficial use of deep ordovician limestone water from mine safety dewatering at the Xinglongzhuang coal mine, north China. Mine Water Environ 39:42–56

Cooper HH, Jacob CE (1946) A generalized graphical method for evaluating formation constants and summarizing well-field history. Eos Trans AGU 27(4):526–534

Davis GM, Horswill P (2002) Groundwater control and stability in an excavation in a magnesian limestone near Sunderland, NE England. Eng Geol 66(1):1–18

DHI-WASY (2017) FEFLOW 7.1 User Manual. DHI-WASY GmbH, Berlin Germany. http://www.feflow.com/uploads/media/users_manual71.pdf. Accessed 5 Mar 2020

Dong D, Sun W, Xi S (2012) Optimization of mine drainage capacity using FEFLOW for the no. 14 coal seam of China's Linnancang coal mine. Mine Water Environ 31:353–360

DZ/T 0285 (2015) Technical guide for mine grout curtains in China. Standards Press of China, Beijing **(in Chinese)**

Guo JF (2005) Problems in exploitation of China complicated hard to mine ore deposit and countermeasures. Met Mine 12:10–13 (**(in Chinese)**)

He K, Wang R, Jiang WF (2012) Groundwater inrush channel detection and curtain grouting of the Gaoyang iron ore mine. China Mine Water Environ 31(4):297–306

Hu YB, Li WP, Wang QQ, Liu SL, Wang ZK (2019) Evaluation of water inrush risk from coal seam floors with an AHP-EWM algorithm and GIS. Environ Earth Sci 78:290–305

Huang F, Wang GH, Yang YY, Wang CB (2014) Overexploitation status of groundwater and induced geological hazards in China. Nat Hazards 73:727–741

Hunt RJ, Steuer JJ, Mansor MTC, Bullen TD (2001) Delineating a recharge area for a spring using numerical modeling, Monte Carlo techniques, and geochemical investigation. Groundwater 39(5):702–712

Leake SA, Claar DV (1999) Procedures and computer programs for telescopic mesh refinement using MODFLOW. Geol Surv Open File Rep, U.S. https://doi.org/10.3133/ofr99238

Liu SL, Li WP (2019) Indicators sensitivity analysis for environmental engineering geological patterns caused by underground coal mining with integrating variable weight theory and improved matter-element extension model. Sci Total Environ 686:606–618

Liu SL, Li WP, Qi W, Li XQ, Wang QQ, He JH (2019) Zoning method for mining-induced environmental engineering geological patterns considering the degree of influence of mining activities on phreatic aquifer. J Hydrol 578:124720

Medeiros WE, Nascimento AFD, Silva FCA, Destro N, Demétrio JGA (2010) Evidence of hydraulic connectivity across deformation bands from field pumping tests: two examples from Tucano Basin, NE Brazil. J Struct Geol 32(11):1783–1791

Mendecki AJ (1997) Seismic monitoring in mines. Chapman & Hall, London

Morris MD (1991) Factorial sampling plans for preliminary computational experiments. Technometrics 33(2):161–174

Murray Darling Basin Commission (MDBC) (2001) Groundwater flow modeling guideline. Report prepared by Aquaterra

Qiao W, Li WP, Li T, Chang JY, Wang QQ (2017) Effects of coal mining on shallow water resources in semiarid regions: a case study in the Shennan mining area, Shaanxi, China. Mine Water Environ 36:104–113

Ta D, Cao S, Steyl G, Yang HY, Li Y (2019) Prediction of groundwater inflow into an iron mine: a case study of the Thach Khe iron mine, Vietnam. Mine Water Environ 38(2):310–324

Theis CV (1935) The relation between the lowering of the piezometric surface and the rate and duration of discharge of a well using groundwater storage. Eos Trans AGU 16(2):519–524

Tzampoglou P, Loupasakis C (2018) Evaluating geological and geotechnical data for the study of land subsidence phenomena at the perimeter of the Amyntaio coalmine, Greece. Int J Min Sci Technol 28:601–612

Wang J, Liu X, Wu YB, Liu SL, Wu LG, Lou RX, Lu JS, Yin Y (2017) Field experiment and numerical simulation of coupling non-Darcy flow caused by curtain and pumping well in foundation pit dewatering. J Hydrol 549:277–293

Ward DS, Buss DR, Mercer JW, Hughes SS (1987) Evaluation of a groundwater corrective action at the Chem-Dyne hazardous waste site using a telescopic mesh refinement modeling approach. Water Resour Res 23(4):603–617

Wu Q, Liu YZ, Wu XL, Liu SQ, Sun WJ, Zeng YF (2016) Assessment of groundwater inrush from underlying aquifers in Tunbai coal mine, Shanxi province, China. Environ Earth Sci 75:737–750

Wu Q, Guo XM, Shen JJ, Xu S, Liu SQ, Zeng YF (2017) Risk assessment of water inrush from aquifers underlying the Gushuyuan coal mine, China. Mine Water Environ 36:96–103

Xue S, Liu Y, Liu S, Li WP, Wu YL, Pei YB (2018) Numerical simulation for groundwater distribution after mining in Zhuanlongwan mining area based on visual MODFLOW. Environ Earth Sci 77:400–409

Yang Z, Li WP, Li XQ, He JH (2019) Quantitative analysis of the relationship between vegetation and groundwater buried depth: a case study of a coal mine district in Western China. Ecol Indic 102:770–782

Zhang GL, Zhan KY, Sui WH (2011) Experimental investigation of the impact of flow velocity on grout propagation during chemical grouting into a fracture with flowing water. J China Coal Soc 36:403–406 (**(in Chinese)**)

Zhang P, Yang T, Yu QL, Xu T, Shi WH, Li SC (2016) Study of a seepage channel formation using the combination of microseismic monitoring technique and numerical method in Zhangmatun iron mine. Rock Mech Rock Eng 49(9):3699–3708

Zhao CH (2013) Analysis on local and overall sensitivity of high pressurized hydrological parameters of aquifer. Coal Sci Technol 41(8):110–113

Zhou N, Vermeer PA, Lou RX, Tang YQ, Jang SM (2010) Numerical simulation of deep foundation pit dewatering and optimization of controlling land subsidence. Eng Geol 114(3–4):251–260